JOURNAL OF APPLIED ELECTROCHEMISTRY 9 (1969) 635–640

The distribution of antimony in the oxide layer formed by potentiostatic oxidation of Pb-Sb alloy

F. ARIFUKU, H. YONEYAMA, H. TAMURA

Department of Applied Chemistry, Faculty of Engineering, Osaka University, Suita, Osaka, Japan

Received 22 September 1978

The distribution of antimony within the oxide films on Pb–Sb alloy prepared by potentiostatic oxidation in H_2SO_4 solutions was examined by SIMS. The study of oxide films prepared by applying different potentials for three hours showed that two types of film were obtained depending on whether the potential was more negative or more positive than 1·5 V. Antimony profiles were obtained for films at several stages in the initial growth. It was found that antimony was retained in the oxide film at 1·5 V during both nucleation and two- or three-dimensional growth of PbO_2 and at 1·6 V during the lateral overlaps of three-dimensional centres of PbO_2. Relationships between the antimony distribution profiles and the oxide film growth are discussed.

1. Introduction

Antimony dissolved anodically from lead–antimony alloy grids [1] plays a beneficial role in the performance of the positive plate in lead–acid batteries [2–4]. Unfortunately, however, the mechanism by which the antimony dissolves is not well known. In order to approach this problem, it seems important to obtain exact information on the behaviour of antimony in anodically oxidized lead–antimony alloys.

In a previous paper, we investigated the macroscopic distribution profiles of antimony in oxide films on a lead–antimony alloy, and revealed that the distribution profile was almost independent of the final polarization potential chosen for the preparation of the films; the films were prepared by multi-triangular potential sweeps. The results obtained, however, showed that it was impossible to get information on the dissolution behaviour of antimony from the well-grown oxide films of the alloy.

In this study, the distribution of antimony as a function of depth was obtained for films formed during the initial stages of potentiostatic oxidation of a lead–antimony alloy. In the potentiostatic oxidation of the alloy, lead dioxide crystals will be formed in several successive steps such as dissolution of the alloy, nucleation, two- or three-dimensional growth of the crystals [5–9]. Fortunately, we can distinguish these steps from the shape of the current–time curves obtained during the oxidation period. In this study, therefore, the main objective was to correlate the distribution profiles with the individual step of the potentiostatic oxidation. Although it has already been shown [10, 11] that the content of antimony in the alloy influences the dissolution behaviour of antimony as well as the oxidation behaviour of lead, the present study was conducted on an alloy of fixed antimony content.

2. Experimental

The preparation of lead–antimony electrodes was described in the previous paper [12]. The content of antimony in the alloy was again 4·92 wt%. Prior to anodic oxidation of the alloy, it was held at $-1{\cdot}2$ V for 30 min to remove completely any oxide film on the alloy. During potentiostatic oxidation of the alloy, current–time curves were recorded, and the charge passed was evaluated from these transients. Samples prepared by potentiostatic oxidation were washed with distilled water for several seconds and then subjected to an in-depth analysis of antimony by using an ion microanalyzer [12]. A mercurous sulphate electrode in 5 M H_2SO_4 was used as the reference electrode. All the other details have already been described [12].

0021–891X/79/050635–06 $02·60/0

3. Results

The current–time curves for the Pb–Sb alloy in 5 M H_2SO_4 obtained during potentiostatic oxidation are shown in Fig. 1. These curves are similar to those obtained in 4·5 M H_2SO_4 by Sharpe [10].

The in-depth analysis of the resulting films shows that the film thickness was almost constant and independent of the charge passed if the film was prepared at potentials less positive than 1·5 V. However, if the oxidation was carried out at potentials more positive to this potential, the film thickness was proportional to the charge passed. These results are given in Fig. 2. The abscissa of this figure is a measure of the film thickness. On the basis of the results shown in Fig. 2, we tentatively classified the oxidation film prepared at various potentials into two groups, denoted here as the A and B groups. The film prepared at potentials less than 1·5 V belong to the A group, and those prepared at potentials more positive than 1·55 V belong to the B group. The classification into these two groups has already been suggested by Sharpe [10]. The results in Fig. 2 seemed to be in agreement with those obtained by weight loss experiments during potentiostatic oxidation [13].

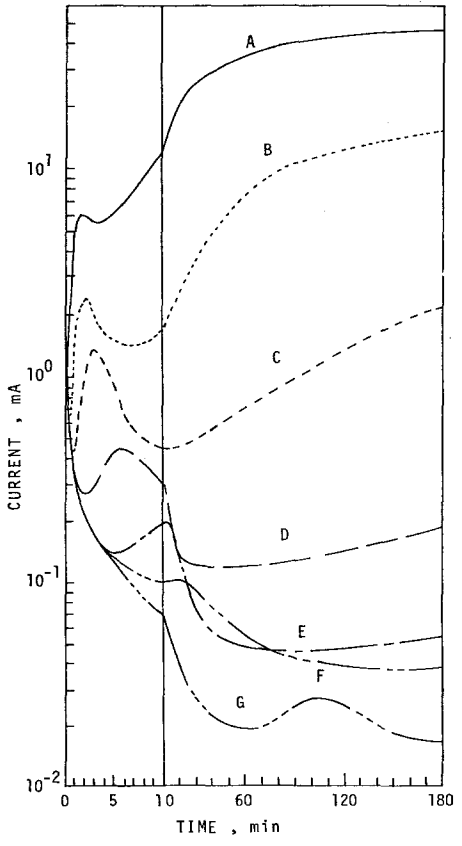

Fig. 1. Current–time curves for potentiostatic oxidation of Pb–Sb alloy in 5 M H_2SO_4 for 3 h. A, 1·65 V; B, 1·60 V; C, 1·55 V; D, 1·50 V; E, 1·45 V; F, 1·40 V; G, 1·30 V versus Hg/Hg_2SO_4 reference electrode.

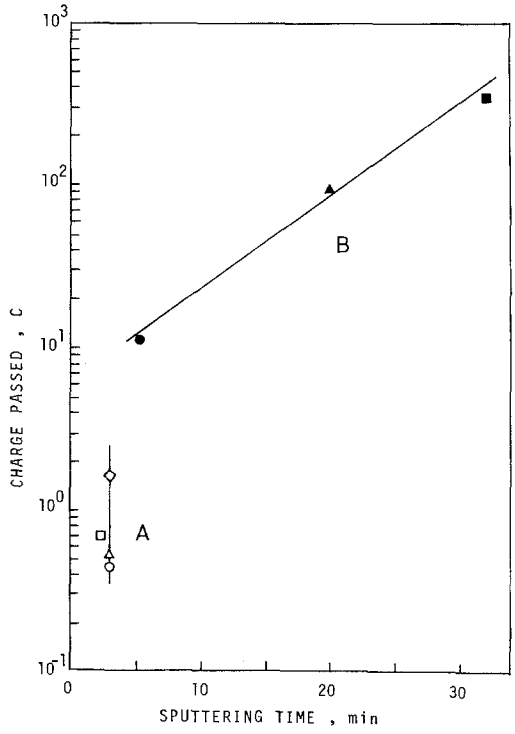

Fig. 2. Relationship between charge consumed in preparation of oxide film and time required for sputtering out the prepared film. ○ 1·30 V; △ 1·40 V; □ 1·45 V; ◇ 1·50 V; ● 1·55 V; ▲ 1·60 V; ■ 1·65 V versus Hg/Hg_2SO_4 reference electrode.

Figs. 3 and 4 show signal intensity ratios I_{rel} (SbO_2^- to PbO_2^-) as a function of sputtering time, for the two groups of films. The solid lines in the figures show the regions where a corrosion layer is observed [12]. It is seen by comparing Fig. 3 with Fig. 4 that the distribution profiles are quite different for the two groups. The relation between I_{rel} and sputtering time (i.e. film thickness) shows a distinct minimum for the A group, but a simple increasing trend for the B group. Furthermore, I_{rel} is larger for the A than for the B group.

In the previous paper, I_{rel} was converted into antimony content in the film by using a calibration curve between I_{rel} and antimony content.

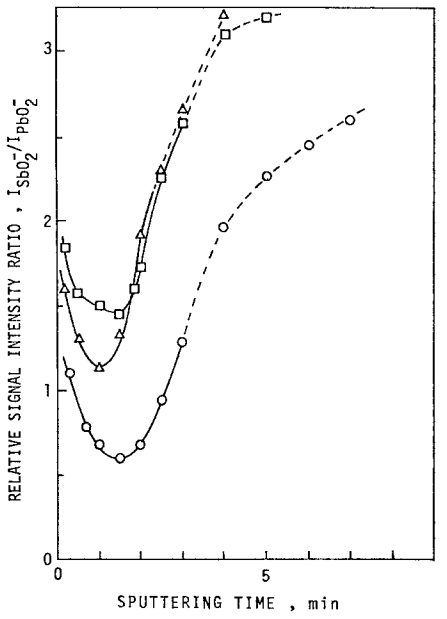

Fig. 3. In-depth profiles of relative signal intensity ratio, $I_{SbO_2^-}/I_{PbO_2^-}$, as a function of sputtering time for films obtained by potentiostatic oxidation. ○ 1·30 V; △ 1·45 V; □ 1·50 V. The solid lines show the regions of the corrosion layer.

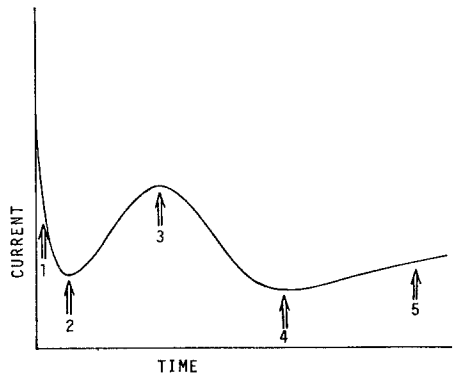

Fig. 5. Schematic representation of the current–time curve for anodic oxidation under potentiostatic control. The arrows indicate five oxidation steps at which specimens were prepared.

When this calibration curve was applied to the present results, however, very high antimony contents were obtained. We therefore feel that the nature of the oxide film is different. In view of this, I_{rel} is used throughout this paper only as a measure of the relative antimony contents in the corrosion film.

In order to study the dissolution behaviour of antimony in the initial stages of the anodic oxi-

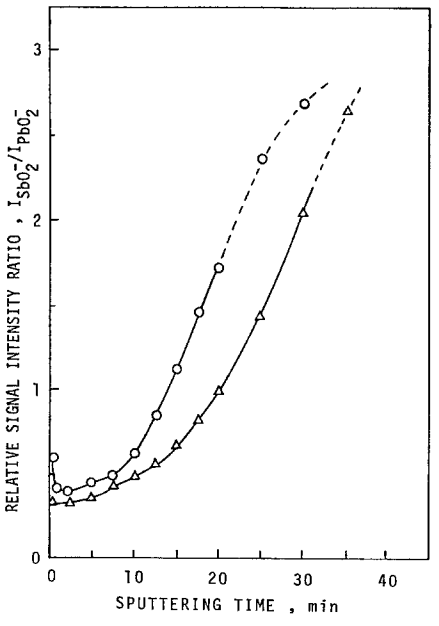

Fig. 4. In-depth profiles of relative signal intensity ratio, $I_{SbO_2^-}/I_{PbO_2^-}$, as a function of sputtering time for films obtained by potentiostatic oxidation. ○ 1·60 V; △ 1·65 V.

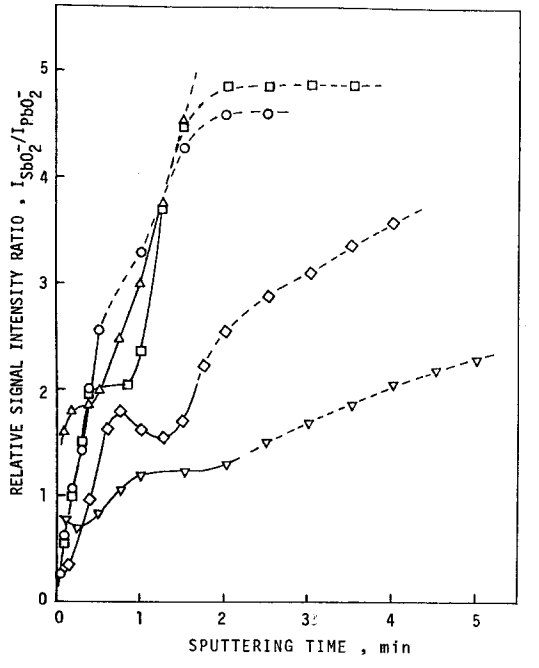

Fig. 6. In-depth profiles of relative signal intensity ratio, $I_{SbO_2^-}/I_{PbO_2^-}$, as a function of sputtering time for films formed at oxidation steps denoted in Fig. 5 for the 1·5 V oxidation case. ○ 1; △ 2; □ 3; ◇ 4; ▽ 5.

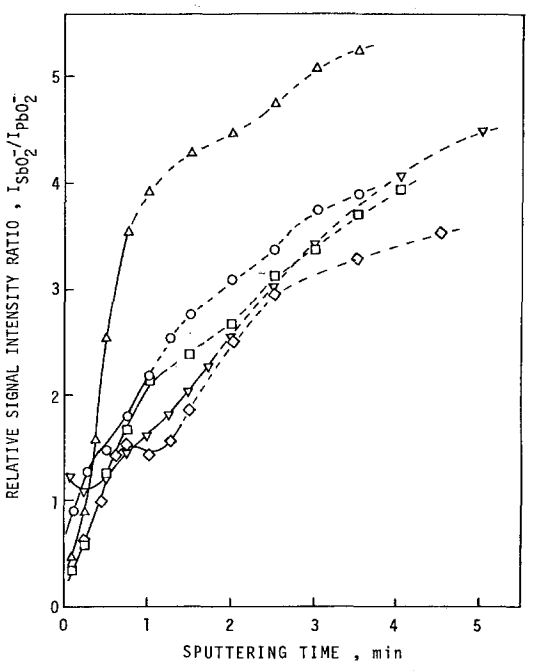

Fig. 7. In-depth profiles of relative signal intensity ratio, $I_{SbO_2^-}/I_{PbO_2^-}$, as a function of sputtering time for films formed at oxidation steps denoted in Fig. 5 for the 1·6 V oxidation case. ○ 1; △ 2; □ 3; ◇ 4; ▽ 5.

dation of the alloy, distribution profiles for antimony were obtained for samples prepared by stopping the oxidation at the times shown with arrows in the current–time curve in Fig. 5. The phenomenon occurring in each oxidation step has already been studied by other investigators [6–8]. The films prepared at 1·5 V and 1·6 V were chosen as representatives of the A and B groups, respectively, and the results are given in Figs. 6 and 7. The following points may be noted from Fig. 6: (a) Step 1; I_{rel} decreased linearly from the alloy substrate to the surface of the film. (b) Steps 2–4; I_{rel} shows plateaux and the location of the plateau moves towards the interior with further oxidation. In the surface region, I_{rel} increased linearly with depth. (c) Step 5; the dependence of I_{rel} on the depth becomes less defined, and I_{rel} began to show only a slight increase with depth. In Fig. 7, slightly different results are noticed for steps 2 and 3. Almost linear dependences on the depth are seen during these stages in the oxidation.

4. Discussion

When the oxidation of the alloy is carried out, the antimony distribution profiles change with time.

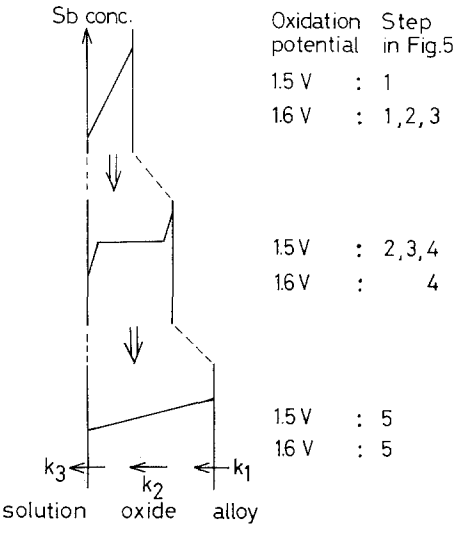

Fig. 8. Classification of obtained profiles into three schematic representations.

In order to understand such changes, it seems appropriate to assume the existence of at least three electrochemical processes in the course of dissolution of antimony into the electrolyte:

(a) ionization of antimony at the alloy–film interface. At this interface, the ionization of lead also occurs.

(b) migration of antimony in the film.

(c) dissolution of antimony from the oxide film region into the bulk electrolyte.

We have no definite evidence for processes (a) and (b), but the profiles obtained are best understood by assuming their existence. If the relative rate constant of the individual processes are denoted as k_1, k_2 and k_3, the profiles in Fig. 8 will be obtained for appropriate values of the hypothetical rate constants, which are also shown in the figure.

Step 1 (in Fig. 5) concerns the dissolution and precipitation of lead, and the profile obtained suggests that the rate of dissolution into the electrolyte bulk, k_3, is larger than the dissolution rate of antimony from the alloy, k_1. This trend holds for films prepared at both 1·5 V and 1·6 V. During steps 2 and 3 the oxidation proceeds (i.e. nucleation and two- and three-dimensional growth of PbO_2 crystals occur) and k_3 becomes relatively small compared to k_1 and k_2 the bulk migration rate constant. In the film prepared at 1·5 V the accumulation of antimony in the film takes place, and I_{rel} becomes independent of charge. The

Table 1. Charge passed up to oxidation step 2 of Fig. 5 in the current–time curves of Fig. 1.

Applied potential (V)	1.30	1.40	1.45	1.50	1.55	1.60	1.65
Charge passed (C)	0.15	0.16	0.05	0.07	0.05	0.03	0.02

decrease of k_3 compared to k_1 and k_2 may reflect the situation where dissolved antimony strongly interacts with oxidized lead.

In the case of the film prepared at 1·6 V, however, the situation is different. The distribution profiles are understandable if k_1 and k_3 are larger than k_2. Certainly k_1 is expected to be larger at this applied potential. With the film formed at 1·5 V, k_3 was thought to be the smallest as described above. Therefore, the question arises as to why k_3 is now large. A plausible answer to this question may be as follows. According to the current–time traces in Fig. 1, the lower the oxidation potential, the longer is the time required to reach step 2. The charge passed before the current–time traces show that step 2 has been reached was also high for the lower oxidation potentials as shown in Table 1. The formation of Pb^{4+} must pass through Pb^{2+}; Pb^{2+} is more stable at the 1·5 V oxidation than the 1·6 V case. Therefore, in the former case, there is more chance for the formation of complex Pb(II) oxides containing antimony, for example as lead meta-antimonate [14]. k_3 then refers to the dissolution of antimony from the complexed oxides. At 1·6 V, the life of the Pb^{2+} may be too short for the complexed oxides to be formed, so that dissolved antimony behaves freely as if there is no interaction with the PbO_2 crystals; k_3 would then be large.

The significance of the appearance of the plateau in the I_{rel}–charge curves during step 4, observed at both 1·5 V and 1·6 V, will be different from that in steps 2 and 3. In step 4, the alloy has just become completely covered by lateral overlaps of three-dimensionally grown PbO_2 crystals. If antimony is anodically dissolved underneath the PbO_2 crystals in the course of steps 3–4, it cannot directly dissolve into the electrolyte. The PbO_2 crystal block the dissolution into the electrolyte. Thus k_3 decreases, and antimony accumulates in the films causing the appearance of the plateau.

During step 5, the oxidation leads to a thick film. In this process, the migration of antimony is the lowest of the three steps. Therefore a monotonic gradient of antimony appears.

Hence, the distribution profiles in Fig. 4 seem to be reasonable. The results shown in Fig. 3, however, are quite different from those expected during step 5 of the oxidation at 1·5 V. If k_3 is quite small, antimony will accumulate in the film surface region and the observed profiles will occur. At present we can give no definite explanation to the observed behaviour, but the profiles may be caused because the removal of antimony only occurs from dense oxide films when the film growth continues. According to the current–time traces of Fig. 1, the charge passed in the 3 h oxidation was dependent on the potential chosen, but the film thickness was not very different when the potential was below 1·5 V (as judged from the in-depth analysis of the films). This phenomenon implies that the film formation was completed in the early stages of the 3 h oxidation. At 1 h the current fell to an almost constant value. Further polarization only leads to oxygen evolution and rearrangement of the ionic configuration of the film, which brings about the accumulation of antimony in the surface region.

It is well known that the presence of antimony in the electrolyte influences the morphology of PbO_2 crystals [2, 15]. Antimony must have some role in the crystallization step (steps 2 and 3). According to the distribution profiles obtained during these steps, more antimony is retained in the oxide films prepared at 1·5 V than at 1·6 V. In the former oxides, the plateau appeared. Therefore, the effects of antimony will be more evident during the oxidation at 1·5 V than at 1·6 V.

Acknowledgements

The authors are grateful to Yuasa Battery Co Ltd and the International Lead Zinc Research Organization, Inc for the financial support of this study.

References

[1] J. Burbank, *J. Electrochim. Soc.* **104** (1957) 693.
[2] *Idem, ibid* **111** (1964) 1112.
[3] D. Kodes, *Chem. Ing. Tech.* **38** (1966) 638.
[4] M. P. J. Brennan, B. N. Stirrup and N. A. Hampson, *J. Appl. Electrochem.* **4** (1974) 49.
[5] P. Ruetschi and R. T. Angstadt, *J. Electrochem. Soc.* **111** (1964) 1323.
[6] P. Casson, N. A. Hampson and K. Peters, *J. Electroanalyt. Chem.* **83** (1977) 87.
[7] *Idem, J. Electrochem. Soc.* **124** (1977) 1655.
[8] E. M. L. Valeriote and L. D. Gallop, *ibid* **124** (1977) 370.
[9] *Idem, ibid* **124** (1977) 380.
[10] T. F. Sharpe, *ibid* **122** (1975) 845.
[11] *Idem, ibid* **124** (1977) 168.
[12] F. Arifuku, H. Yoneyama and H. Tamura, *J. Appl. Electrochem.* **9** (1979) 631.
[13] J. J. Lander, *J. Electrochem. Soc.* **98** (1951) 213.
[14] D. E. Swets, *ibid* **120** (1973) 925.
[15] E. J. Ritchie and J. Burbank, *ibid* **117** (1970) 229.